Northumbria Research Link

Northumbria University NEWCASTLE

UniversityLibrary

Highly luminescent dinuclear platinum(II) complexes incorporating bis-cyclometallating pyrazine-based ligands: a versatile approach to efficient red phosphors

Stacey Culham,[†] Pierre-Henri Lanoë,[†] Victoria L. Whittle,[‡] Marcus C. Durrant,[†]
J. A. Gareth Williams,[‡*] and Valery N. Kozhevnikov[†*]

† School of Life Sciences, Northumbria University, Newcastle upon Tyne, NE1 8ST, U.K.
‡ Department of Chemistry, Durham University, Durham, DH1 3LE, U.K.

_____

Abstract

A series of luminescent dinuclear platinum(II) complexes incorporating diphenylpyrazine-based bridging ligands (L^n) have been prepared. Both 2,5-diphenylpyrazine (n = 2) and 2,3-diphenylpyrazine (n = 3) are able to undergo cyclometallation of the two phenyl rings, with each metal ion binding to the two nitrogen atoms of the central heterocycle, giving, after treatment with the anion of dipivaloyl methane (dpm), complexes of the formula $\{Pt(dpm)\}_2L^n$. These compounds are isomers of the analogous complex of 4,6-diphenylpyrimidine (n = 1). Related complexes of dibenzo(f,h)quinoxaline (n = 4), 2,3-diphenyl-quinoxaline (n = 5) and dibenzo[3,2-a:2',3'-c]phenazine (n = 6) have also been prepared, allowing the effects of strapping together the phenyl rings (n = 4 and 6) and/or extension of the conjugation from pyrazine to quinoxaline (n = 5 and 6) to be investigated. In all cases, the corresponding mononuclear complexes, Pt(dpm)L^nH, have been isolated too. All 12 complexes are phosphorescent in solution at ambient temperature. The emission spectra of the dinuclear complexes are consistently red-shifted compared to their mononuclear analogues, as are the lowest-energy absorption bands. Electrochemical data and TD-DFT calculations suggest that this effect arises primarily from a stabilisation of the LUMO. The introduction of the second metal ion also has the effect of substantially increasing extinction coefficients in absorption, and − in most cases − the radiative rate constants. Meanwhile, the extension of conjugation in the heterocycle of L^5 and L^6, and planarisation of the aromatic system favoured by interannular bond formation in L^4 and L^6, leads to further red shifts of the absorption and emission spectra to wavelengths that are unusually long for cyclometallated platinum(II) complexes. The results may offer a versatile design strategy for tuning and optimizing the optical properties of d-block metal complexes for contemporary applications.

_____

[†] Northumbria University. E-mail: valery.kozhevnikov@northumbria.ac.uk
[‡] Durham University. E-mail: j.a.g.williams@durham.ac.uk

Introduction

Phosphorescent red and near-infrared emitters are desired for a variety of applications. For example, in the field of light-harvesting phosphors for organic light-emitting diodes (OLEDs) and light-emitting electrochemical cells (LECs), red emitters are required for full-colour displays and for white-light systems destined for lighting applications.[1,2,3] Yet the currently available red-emitting compounds are not able to match the high performance of green emitters.[4] Meanwhile, in the field of luminescent sensors for bioimaging and sensing,[5] there is a need for compounds that not only emit in the red or near infrared (NIR) regions, but also *absorb* at long wavelengths, in order to benefit from the window of greater optical transparency of biological tissue and decreased scattering, which favours the delivery and collection of light.[6] There is a similar pressing need for red and NIR-absorbing materials in the development of new dyes for dye-sensitized solar cells (DSSCs), where more efficient collection of light from this region of the solar spectrum is required if efficiencies are to be significantly improved.[7]

One of the most studied classes of phosphorescent materials are Ru(II) complexes of polypyridines, since they often emit in the red region – albeit with modest quantum yields of a few % – from low-energy ^{3}MLCT transition states.[8] More recently, cyclometallated complexes of the phenylpyridine type have become increasingly popular, particularly with third-row metals such as iridium(III)[9,10] and platinum(II).[11,12] The combination of (i) a strong σ donor in the C^- ligating unit that raises the energy of metal-centred orbitals thus stabilizing the MLCT states, (ii) a strong ligand field that destabilizes potentially deactivating d–d states, and (iii) efficient spin-orbit coupling (SOC) induced by the heavy metal ion to promote radiative decay of the triplet state,[13] renders many such complexes very intensely luminescent. Moreover, the emission energy can be quite easily tuned over a wide range by systematic modifications to the ligand, owing to the HOMO and LUMO being localised on mutually different parts of the molecule.[14] In order to shift to the red region of the spectrum, the usual approaches are: (i)

to lower the LUMO energy through the use of a more electron-deficient heterocycle such as an isoquinoline,[4b,c,e,15] (ii) to raise the energy of the HOMO using a more electron-rich aromatic unit such as a benzothiophene,[16] and (iii) to extend the conjugation within the ligand such that the HOMO–LUMO gap decreases.[17] The problem with these approaches, particularly (ii) and (iii), is that, as the ligand-based filled orbitals rise in energy, the amount of metal character in the excited state concomitantly decreases, so that one can expect less efficient SOC, smaller radiative decay constants, and even fluorescence from the ligands due to retarded intersystem crossing.[18] For example, the introduction of additional pendent thiophene groups into thienylpyridine complexes of iridium and platinum leads to a switch from efficient phosphorescence to fluorescence accompanied by only very weak – albeit red-shifted – phosphorescence.[19]

An emerging alternative approach to achieve red-shifted emission is to introduce two or more metal centers into one molecule, by means of a bridging ligand. For example, Zhong and Abruña recently demonstrated that the combination of Pt(II) and Ru(II) metal centers, linked through a dipyridyldiphenylpyrazine bridging ligand, can provide deep red and NIR emitters, albeit with low quantum yields of the order of 10^{-3} or less.[20] We have been interested in the design of new luminescent materials based on polynuclear assemblies with cyclometallated metal centers. Recently, we reported a versatile strategy to access efficient red emitters based on polynuclear Pt(II) and heterometallic Pt(II) / Ir(III) complexes, in which 4,6-di(4-*tert*-butyl-phenyl)pyrimidine was used as the bridging ligand.[21] The general observation was that the introduction of a second cyclometallated metal centre is accompanied by a significant red shift in absorption and emission, mainly due to stabilisation of the LUMO level. Motivated by these results, we sought to extend the methodology to other systems based on related pyrazine rather pyrimidine bridging ligands. We describe here the synthesis of five dinuclear platinum(II) complexes based on diphenylpyrazine-based bridging ligands, together with

their mononuclear analogues. We show how the approach leads to efficient deep-red emission, and explore the influence of isomerism and extended conjugation / rigidification in the bridging ligand.
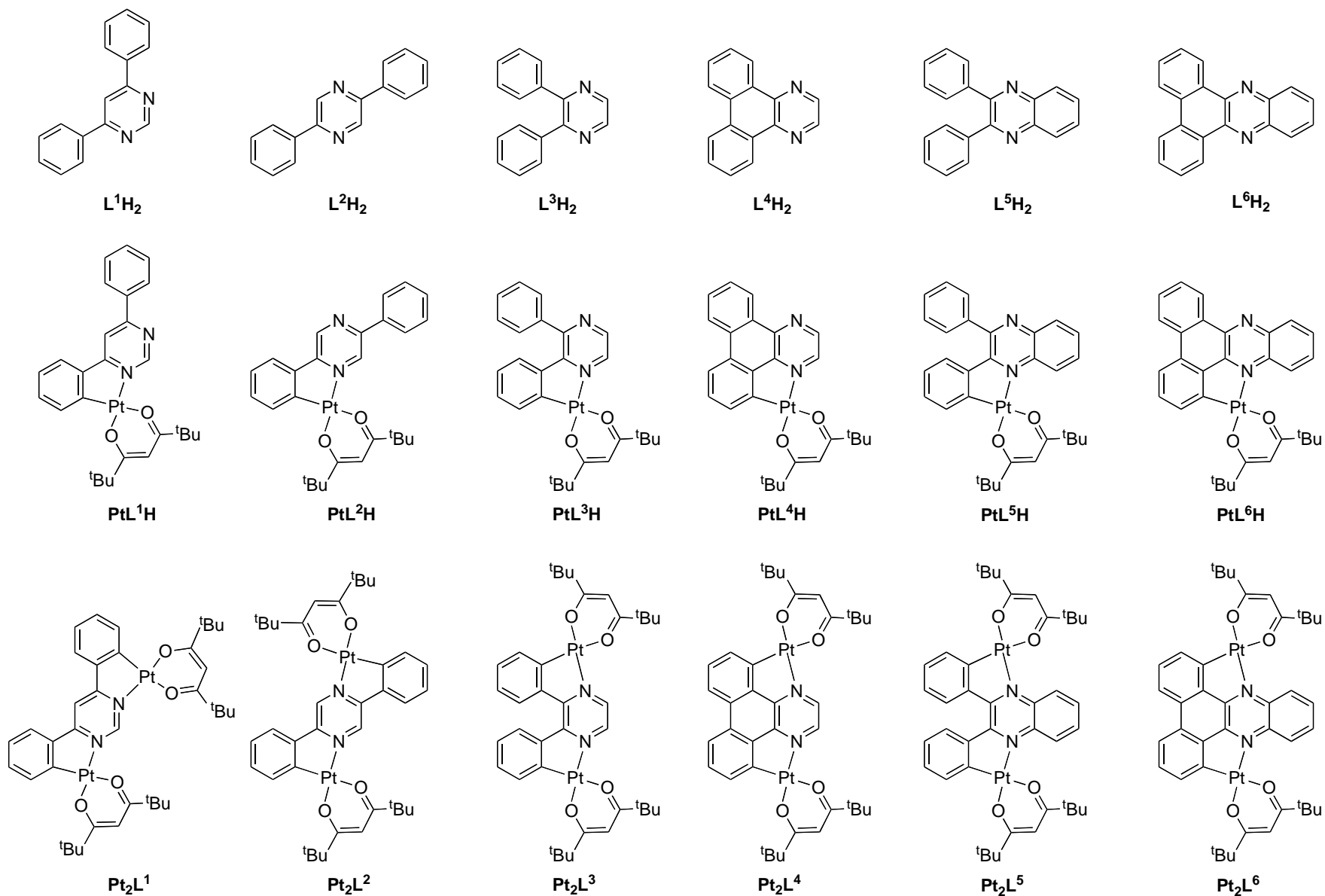
Results and discussion

1. Synthesis

The family of mono- and di-nuclear complexes investigated is shown in Figure 1, together with the corresponding proligands. PtL^1H and Pt_2L^1 are derived from 4,6-diphenylpyrimidine, and are essentially the same as the complexes we reported previously,[21] except that the phenyl rings do not incorporate *tert*-butyl substituents, and dipivaloylmethane (dpm) is used as the ancillary ligand in place of acetylacetonate (acac). The change from acac to dpm allows the complexes to retain good solubility without the need for *tert*-butyl groups in the cyclometallating ligands, facilitating comparison with the new compounds. All the other complexes are based on a diphenylpyrazine core, cyclometallated either once (mononuclear series, PtL^2H – PtL^6H) or twice (dinuclear series, Pt_2L^2 – Pt_2L^6). L^4H_2 is dibenzo(f,h)quinoxaline, L^5H_2 is 2,3-diphenylquinoxaline, and L^6H_2 is dibenzo[3,2-a:2',3'-c]phenazine. Note that the compounds based on L^1, L^2, and L^3 are isomers of one another, so that a direct comparison can be made of the influence of (i) changing from pyrimidine to pyrazine (L^1 versus L^2/L^3), and (ii) the substitution pattern in the pyrazine ring (2,5-substitution in L^2 versus 2,3-substitution in L^3). Meanwhile, it may be seen that the complexes of ligands L^3–L^6 form a series of closely related complexes in which either a C–C bond is introduced between the two pendent phenyl rings (L^4 versus L^3), or the pyrazine is replaced by a quinoxaline (L^5 versus L^3), whilst the complexes of L^6 incorporate both these features.

2,3-Diphenylpyrazine (L^3H_2) and 2,3-diphenylquinoxaline (L^5H_2) are commercially available, whilst the other proligands were prepared by following established procedures (details and references are

given in the Experimental Section). The monometallic Pt(II) complexes, Pt(*N^C*-LH)(dpm) (which will be henceforth be abbreviated as PtL^{n}H) were obtained by heating at reflux a mixture of the proligand and one equivalent of K_2PtCl_4 in acetic acidfor up to 3 days. The resulting dichloro-bridged dinuclear intermediates were then reacted with dipivaloylmethane in the presence of base to give, after purification by column chromatography, the monoplatinum complexes PtL^{n}H in low to moderate yield. The formation of a small amount of the corresponding diplatinum complexes was registered in each case.

The dinuclear platinum(II) complexes (which will be referred to as Pt_2L^n) were synthesised either by reaction of PtL^{n}H with one equivalent of K_2PtCl_4 or by reacting L^{n}H$_2$ with two equivalents of K_2PtCl_4. Under these conditions, it was found that, although the dinuclear complex was the main product, the corresponding monoplatinum complex PtL^{n}H was still present in the mixture. In general, it proved to be most convenient to prepare the two complexes simultaneously by reaction of the proligand L^{n}H$_2$ with 1.5 equivalents of K_2PtCl_4, targeting a statistical 1:1 mixture. After introduction of the dpm ancillary ligand under conventional conditions, the mono- and dinuclear platinum complexes are readily separated by column chromatography (typically on silica gel eluting with dichloromethane) to give both products in one procedure. All products were characterised by ^{1}H NMR spectroscopy, mass spectrometry and elemental analysis.

Figure 1 *Structures of the proligands, $L^n H_2$, mono-nuclear platinum(II) complexes, $PtL^n H$, and dinuclear platinum(II) complexes, $Pt_2 L^n$*

$L^1 H_2$	$L^2 H_2$	$L^3 H_2$	$L^4 H_2$	$L^5 H_2$	$L^6 H_2$
$PtL^1 H$	$PtL^2 H$	$PtL^3 H$	$PtL^4 H$	$PtL^5 H$	$PtL^6 H$
$Pt_2 L^1$	$Pt_2 L^2$	$Pt_2 L^3$	$Pt_2 L^4$	$Pt_2 L^5$	$Pt_2 L^6$

2. Electrochemistry

The electrochemical behaviour of the complexes was examined by cyclic voltammetry in dichloromethane solution, using Bu_4NPF_6 as the supporting electrolyte and the ferrocene/ferrocenium couple as the reference. All twelve complexes display one reversible or quasi-reversible reduction wave, in the range –2.2 to –1.4 V versus ferrocene; the reduction potentials are given in Table 1. Four trends emerge upon inspection of the data:

(i) For any given ligand L^n, the reduction potential of the dinuclear complex Pt_2L^n is significantly less negative than for the corresponding mononuclear complex PtL^nH, by around 200–300 mV.

(ii) Amongst the three isomeric complexes PtL^1H–PtL^3H, there is little difference between the reduction potentials, all being within 80 mV. Similarly, the three dinuclear complexes of these ligands have reduction potentials that are within 40 mV of one other. Apparently, then, the change from pyrimidine to pyrazine has rather little effect on the reduction, as does the substitution pattern within the pyrazine.

(iii) Strapping together the two phenyl rings in the 2,3-substituted pyrazine system (PtL^4H versus PtL^3H, and Pt_2L^4 versus Pt_2L^3) facilitates reduction by around 100 mV, with a qualitatively similar effect in the quinoxaline analogues (L^6 versus L^5).

(iv) The change from pyrazine to quinoxaline (complexes of L^5 versus L^3, and of L^6 versus L^4) is accompanied by a more significant anodic shift of the reduction, of the order of 300 mV.

Trends (i), (iii) and (iv) are consistent with the intuitively reasonable notion that the LUMO in such complexes {which would be expected to be essentially ligand-based, according to previous experimental and theoretical work on cyclometallated Pt(II) complexes[11,12]} will be stabilised by the extension of conjugation that accompanies (i) the introduction of the second metal ion, (ii) the incorporation of the interannular bond which facilitates a planar conformation, and (iii) the change from pyrazine to quinoxaline.

Table 1 UV-visible absorption data and ground-state reduction potentials for the complexes[a]

Complex	λ_{max} / nm (ε / $M^{-1}cm^{-1}$)	E^0_{red} / V [ΔE / mV]
PtL^{1}H	256 (25200), 301 (31600), 338sh (10600), 408 (9550)	−2.21 [160]
Pt$_2$L^1	257 (47000), 326 (63200), 430 (17100), 481 (24300), 532sh (1990)	−1.83 [160]
PtL^{2}H	254 (26800), 299 (25400), 342 (17300), 398 (6430), 435 (5240)	−2.13 [180]
Pt$_2$L^2	253 (35300), 296 (26500), 333 (21900), 372 (16600), 453 (15900), 503 (6830), 618 (346)	−1.79 [100]
PtL^{3}H	252 (23800), 292 (16900), 340 (11900), 398 (6170), 449 (2170)	−2.14 [150]
Pt$_2$L^3	245 (36700), 301 (20300), 319 (20700), 390 (19600), 451 (15200), 572 (310)	−1.81 [90]
PtL^{4}H	251 (66000), 278 (42100), 344 (18900), 407 (11800), 463 (3190)	−2.02 [150]
Pt$_2$L^4	258 (59300), 295 (25900), 308 (25700), 350 (25800), 428 (10100), 462 (19400), 509 (11500)	−1.70 [120]
PtL^{5}H	252 (40000), 294 (20000), 373sh (9380), 388 (10600), 445 (6470), 488sh (3790)	−1.83 [100]
Pt$_2$L^5	251 (42000), 313 (21600), 387 (14200), 428 (8610), 496 (1360)	−1.46 [90]
PtL^{6}H	251 (52300), 282 (38000), 383sh (7870), 401 (10300), 463 (7790), 511 (4520)	−1.66 [90]
Pt$_2$L^6	266 (29000), 301sh (13600), 324sh (11500), 396 (3070), 422 (3890), 476sh (3350), 519 (7780), 569 (6690)	−1.43 [90]

(a) In CH$_2$Cl$_2$ at 298 ± 3 K. Reduction potentials obtained by cyclic voltammetry, using Bu$_4$NPF$_6$ (0.1 M) as the supporting electrolyte. Potentials are given relative to the Fc|Fc$^+$ couple measured under the same conditions. The peak-to-peak separation is given in parentheses.

As is typically found for cyclometallated platinum(II) complexes, the first oxidation process observed for each of the complexes studied was irreversible and, in several cases, rather ill-defined. Indeed, we found an unsatisfactory level of variation in the peak potential according to the conditions, not only of the scan rate, but even from one scan to the next, despite extensive cleaning of the electrode surface between scans. However, the data showed unequivocally that there is significantly less variation in the oxidation potentials with molecular structure than in the reduction potentials: the values were generally

around 0.8 V versus Fc|Fc$^+$, a value quite typical for cyclometallated platinum complexes with arylpyridine ligands.

3. Absorption spectroscopy

Absorption data for all 12 complexes is compiled in Table 1, and spectra are shown in Figures 2 and 3. In order to facilitate the discussion, we shall first consider the behaviour of the two sets of three isomeric complexes, PtL$^{1-3}$H and Pt$_2$L$^{1-3}$, and then examine how the elaboration of the L^3 ligand influences the properties on moving to the complexes of ligands L$^{4-6}$. The mononuclear complexes PtL$^{1-3}$H display absorption spectra that are quite typical of platinum(II) complexes with N^C-cyclometallating, aryl-heterocycle ligands, such as Pt(ppy)(acac) and related derivatives.[11,12] There are intense bands in the UV region, < 350 nm, with extinction coefficients ε in the range 10 000 – 30 000 M^{-1}cm^{-1}, corresponding to ^{1}π–π* transitions associated with the ligands (Figure 2, Table 1). Somewhat weaker bands, ε < 10 000 M^{-1}cm^{-1}, in the visible region (390 – 500 nm) have no counterparts in the free proligands. Based on the conclusions of many previous studies,[12] and on the results of time-dependent density functional theory calculations for the present series of complexes (*vide infra*), at least some of these bands can be attributed to charge-transfer transitions from the aryl–metal unit to the heterocyclic ring, reflecting the predominant localisation of the frontier orbitals on these two different parts of the molecule.

The dinuclear complexes Pt$_2$L$^{1-3}$ display very different spectra from their corresponding mononuclear analogues PtL$^{1-3}$H (Figure 2, Table 1). For the complexes of L^1 and L^2, the set of lower-energy bands in the visible region are substantially red-shifted in the dinuclear compared to the mononuclear complexes (lowest-energy band shifts by around 4000 cm^{-1}), and there is a large increase in the extinction coefficients of most of the bands. The visible-region bands in Pt$_2$L^3, on the other hand, are

scarcely shifted compared to PtL^{3}H, although there is again a very large increase in the extinction coefficients. The red-shift in the dinuclear complexes of L^1 and L^2 is likely to be associated with the planarization and extension of conjugation that would be expected to accompany the introduction of the second metal ion. In the case of Pt$_2$L^3, on the other hand, it seems likely that the attainment of a fully planar structure will be inhibited by steric crowding of the C–H bonds of the pendent phenyl groups, which would account for the lack of red shift in that case.
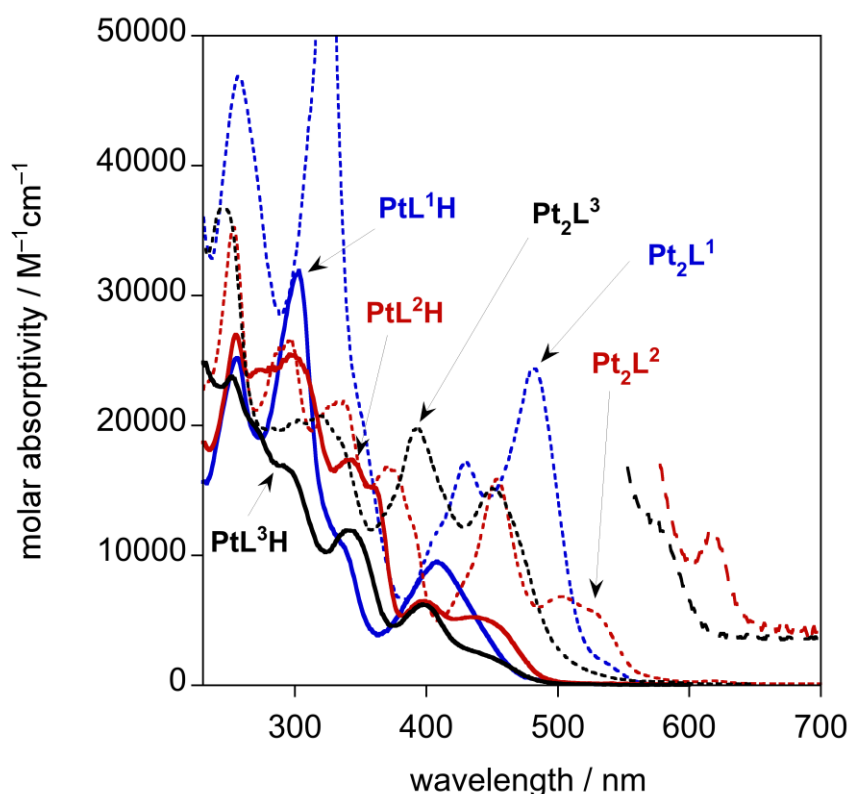
Figure 2 *UV-visible absorption spectra of PtL$^{1-3}$H (blue, red, and black solid lines respectively) and of Pt$_2$L$^{1-3}$ (blue, red, and black short-dashed lines respectively) in CH$_2$Cl$_2$ solution at 298 K. The low-energy region of the spectra of Pt$_2$L^2 and Pt$_2$L^3 is shown on an arbitrarily expanded scale (red and black long-dashed lines respectively).*

A further feature of the dinuclear complexes is the appearance of a very weak transition on the low-energy side of the main bands. In Pt$_2$L^1 and Pt$_2$L^3, it appears as a shoulder (λ = 532 and 572 nm respectively), but for Pt$_2$L^2, as a well-defined narrow band (λ_{max} = 618 nm) (shown on an expanded

scale in Figure 2). It is likely that these bands are due to direct excitation to the triplet state ($S_0 \rightarrow T_1$), a formally forbidden process that is facilitated by the spin-orbit coupling associated with the presence of the heavy metal ions.[xxii]

The absorption spectra of all the other complexes, $PtL^{4-6}H$ and Pt_2L^{4-6}, are shown in Figure 3, together with those of PtL^3H and Pt_2L^3 again as a point of comparison. Considering first the mononuclear complexes, it can be seen that all four display spectra that are quite similar to one another in form, but the visible-region bands move progressively further to the red. The displacement is small on going from PtL^3H to PtL^4H (~700 cm^{-1}), but nevertheless the trend would be consistent with the planarization of the structure that becomes possible upon formation of the interannular C–C bond and loss of the sterically unfavourable interaction between the C–H bonds on the two rings mentioned above. A much larger red-shift accompanies the change from the pyrazine unit of PtL^3H to the quinoxaline of PtL^5H (around 1800 cm^{-1} for the lowest-energy band, and around 2600 cm^{-1} for the next lowest). This trend is consistent with the trend in reduction potentials, which suggests a significant stabilisation of the lowest unoccupied molecular orbital on going from the pyrazine to the quinoxaline, and hence – if the filled orbitals are not substantially lowered in energy – an expected red shift in the lowest-energy absorption band. Indeed, the energy of the lowest-energy absorption maxima for the mononuclear complexes correlates well with the reduction potentials (Figure 4, top, data points represented by blue circles). Notably, PtL^6H and Pt_2L^6, which feature both the interannular bond *and* the quinoxaline unit, display the lowest-energy absorption bands amongst the two series of complexes (mononuclear and binuclear respectively), indicating a qualitatively additive effect.

Again, it is clear that the introduction of the second metal ion leads to a red-shift in the visible-region bands, and to a large increase in the molar absorptivity of these bands. The correlation between the

energy of the absorption maxima and the reduction potentials for the set of complexes as a whole, including the binuclear complexes, remains quite clear, albeit with rather more scatter than for the series of mononuclear complexes alone (Figure 4, top, all data points).
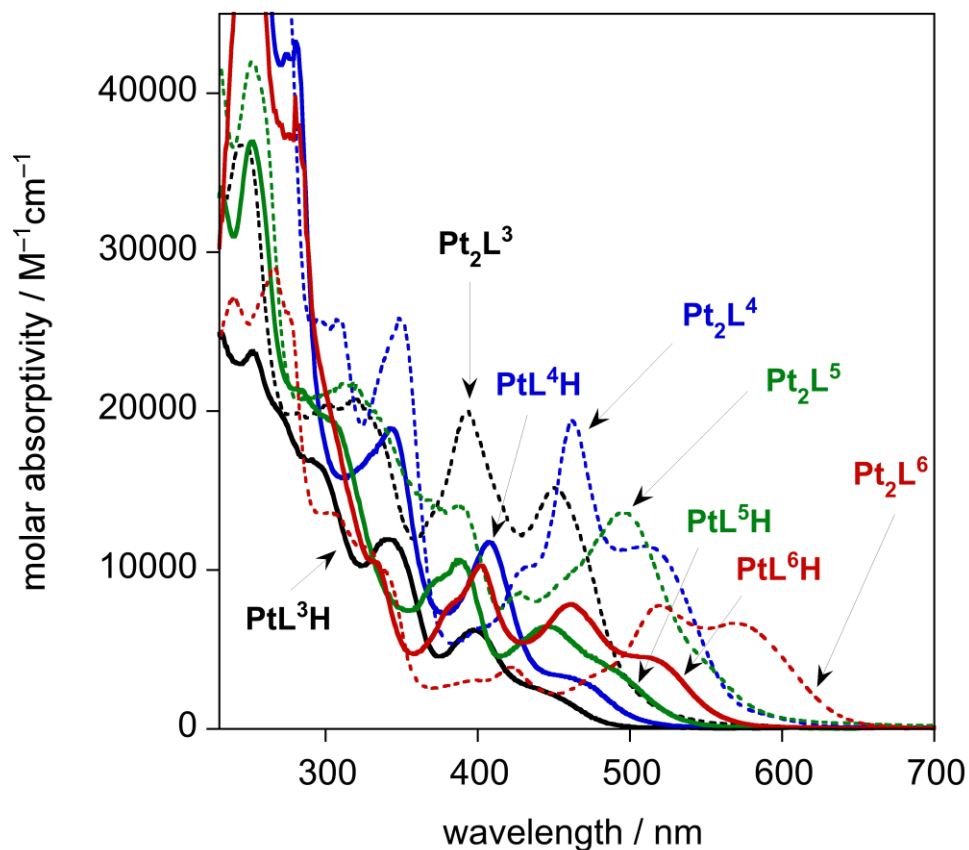
Figure 3 *UV-visible absorption spectra of PtL$^{3–6}$H (black, blue, green, and red solid lines respectively) and of Pt$_2$L$^{3–6}$ (correspondingly coloured dashed lines) in CH$_2$Cl$_2$ solution at 298 K.*
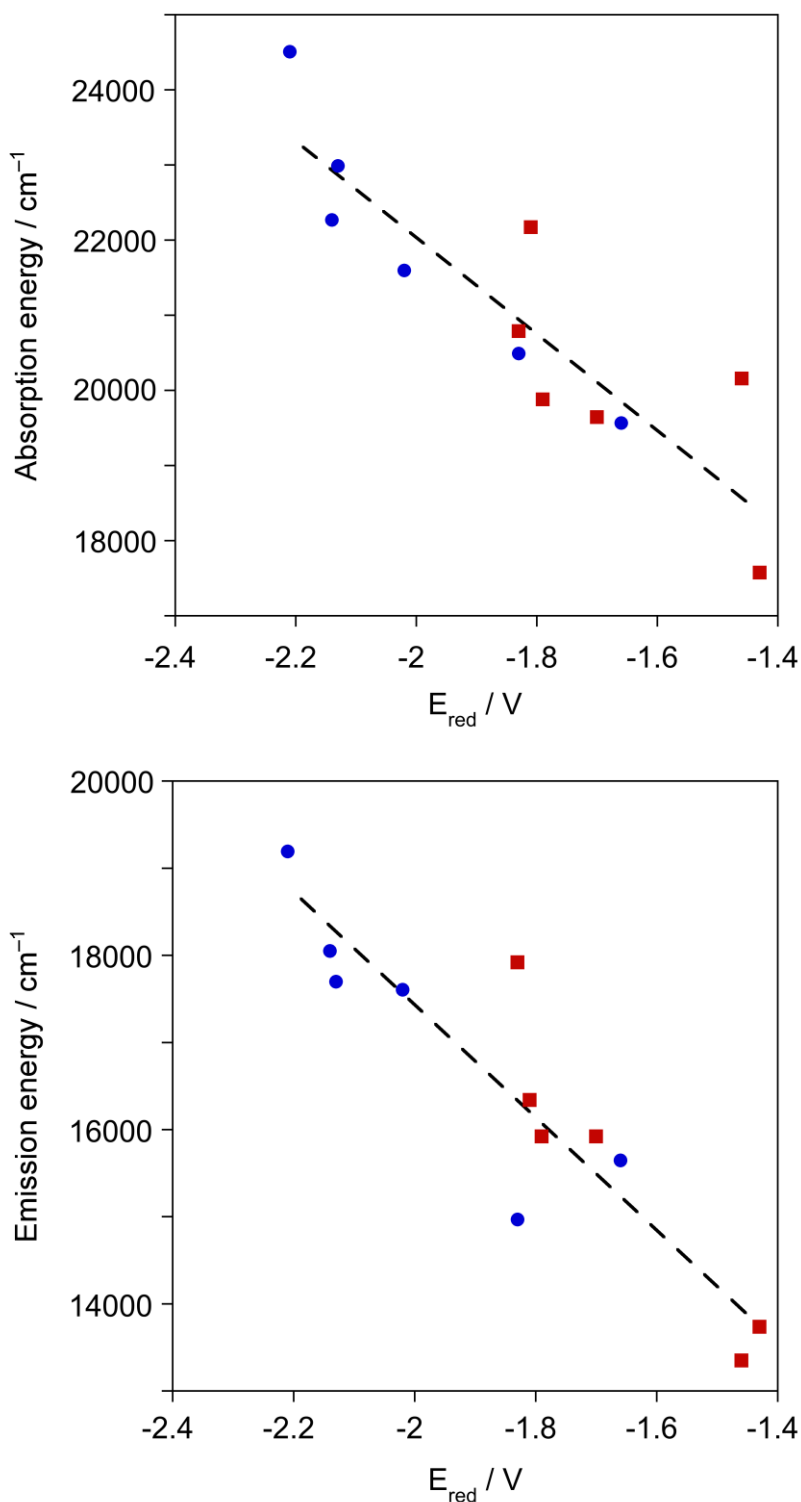
Figure 4 *Top: Plot of the energy of the lowest-energy absorption maximum in CH$_2$Cl$_2$ at 298 K (derived from λ_{max}) versus the reduction potential (values versus Fc/Fc$^+$) obtained by cyclic voltammetry. Data for the mononuclear complexes are shown as blue circles, and for the binuclear complexes as red squares. The dashed line represents the best fit of the data for all 12 complexes; gradient = 6410 cm^{-1}/V. Bottom: Corresponding plot for the emission maximum under the same conditions; gradient of best-fit line = 6460 cm^{-1}/V.*

4. Photoluminescence properties

All twelve complexes are luminescent in degassed solution at room temperature, most of them intensely so. The emission data for the compounds are compiled in Table 2, and the spectra are shown in Figures 5 and 6. The trends in emission maxima are mostly quite similar to those observed in the absorption spectra. In particular, it may be immediately seen that, for a given ligand, the spectrum of the binuclear complex Pt_2L^n is significantly red-shifted compared to that of the corresponding mononuclear complex PtL^nH. The shift is in the range $1600 – 1900$ cm^{-1} for the five pairs of pyrazine-based complexes (based on the emission maxima), and a little less, 1270 cm^{-1}, for the pyrimidine pair (PtL^1H and Pt_2L^1). Overall, there is again a quite strong correlation between the emission energy and the reduction potential of the complexes (Figure 4, bottom), suggesting that the structural variations amongst the complexes predominantly influence the LUMO. The gradient of the best-fit line is very similar to that in the plot for absorption, indicating that the emissive triplet state has similar orbital parentage to the lowest-energy singlet state formed upon absorption.

Amongst the three isomeric complexes $PtL^{1-3}H$, the pyrimidine complex PtL^1H emits at higher energy ($\lambda_{max} = 520$ mm), while the two pyrazine complexes emit in a similar region to one another, with PtL^2H displaying a more structured profile. Meanwhile, the trend amongst the four complexes $PtL^{3-6}H$ is similar to that in absorption, except that PtL^5H emits at marginally *lower* energy than PtL^6H – the opposite of the trend in absorption – and its spectrum is markedly broader. If we consider the difference in energy between the lowest-energy absorption maximum and the emission band {which we will refer to as $\Delta E^{A–E}$; note that it is not strictly a Stokes' shift, since the absorption is to the singlet state whereas the emission occurs from a triplet state}, it can be seen that this value is largest for PtL^5H amongst the mononuclear complexes, and particularly compared to PtL^6H, suggesting that there is a

more profound excited-state reorganisation in this complex prior to emission. We return to this point below.

Two such instances of a reversal in the relative order of emission energies versus absorption energies are observed amongst the binuclear complexes. Thus, Pt_2L^3 emits at significantly lower energy than Pt_2L^1, contrary to the absorption being significantly lower in energy for the latter. Indeed, we noted in Section 3 that Pt_2L^3 seemed somewhat anomalous in that its lowest-energy absorption band was not significantly shifted compared to that of its mononuclear analogue, and we tentatively attributed this to a lack of planarity in the ground state. This complex may undergo a more profound change in geometry towards planarity prior to emission, to lead to a lower-energy triplet excited state from which emission occurs. The second instance is the pair of complexes Pt_2L^5 and Pt_2L^6, where the emission of the former has a slightly longer λ_{max}, despite having an absorption maximum at an unequivocally higher energy. Note that the order is switched round in the more rigid medium of the glass at 77 K (compare Figure 6 top and bottom). Excited-state reorganisation at room temperature can be anticipated for Pt_2L^5 similar to that proposed for Pt_2L^3, given the expected sterically unfavourable interannular interactions in the ground state. In line with this explanation, it is notable that ΔE^{A-E} is larger for these two complexes than for any others.

At 77 K, the emission spectra show otherwise similar trends as at room temperature but the spectra become more vibrationally resolved. The observed vibrational spacing is around $1200 - 1400 \text{ cm}^{-1}$, as typically expected for coupling to aromatic ring vibrations.

Table 2 Emission data for the complexes in degassed CH_2Cl_2 at 298 K except where stated otherwise

Complex	λ_{max} / nm	Φ_{lum} [a]	τ / ns [b]	k_Q^{SQ} [c] / 10^7 M^{-1}s^{-1}	k_r [d] / 10^4 s^{-1}	Σk_{nr} [d] / 10^4 s^{-1}	k_Q^{O2} [e] / 10^8 M^{-1}s^{-1}	ΔE^{A-E} [f] / cm^{-1}	Emission at 77 K [g] λ_{max} / nm	τ / μs
PtL^{1}H	521	0.25	1600 [460]	87	16	47	7.0	5320	501, 527, 573sh	6.4
Pt$_2$L^1	558, 594	0.36	1100 [670]	[h]	33	58	2.6	2870	539, 582, 630	4.3
PtL^{2}H	565, 608	0.30	8900 [840]	71	3.4	7.9	4.9	5290	554, 603, 654	11
Pt$_2$L^2	628, 685, 753	0.41	3200 [680]	[h]	13	18	5.3	3960	617, 676, 742	3.4
PtL^{3}H	554, 578	0.43	7700 [850]	210	5.6	7.4	4.8	4220	536, 576, 618	11
Pt$_2$L^3	612	0.37	4000 [750]	3.5	9.3	16	4.9	5830	586, 634, 693	6.1
PtL^{4}H	568	0.15	2600 [510]	270	5.8	33	7.2	3990	528, 566, 615	11
Pt$_2$L^4	628	0.20	1800 [650]	27	11	44	4.5	3720	601, 654, 716	7.0
PtL^{5}H	668	0.14	3700 [700]	15	3.8	23	5.3	5520	625, 677, 747sh	5.7
Pt$_2$L^5	749	0.025[i]	910 [490]	[h]	2.7[i]	110	4.3	6810	694, 760	3.5
PtL^{6}H	639, 686	0.13	3800 [700]	180	3.4	23	5.3	3920	617, 676, 746	1.3
Pt$_2$L^6	728, 799	0.027[i]	2000 [580]	[h]	1.4[i]	49	5.6	3840	712, 793	1.5

(a) Measured using [Ru(bpy)$_3$]Cl$_2$ as the standard. *(b)* Values in air-equilibrated solution in parenthesis. *(c)* Self-quenching rate constant, estimated from a plot of τ^{-1} versus concentration. *(d)* k_r and Σk_{nr} are the radiative and non-radiative decay rate constants, estimated from the quantum yield and lifetime assuming that the emissive state is formed with unitary efficiency. *(e)* Bimolecular rate constant for quenching by O$_2$, estimated from the luminescence lifetimes in degassed and air-equilibrated solutions, and taking [O$_2$] = 2.2 mM in CH$_2$Cl$_2$ at p = 1 atm air and T = 298 K. *(f)* The difference between the energy of the lowest-energy (singlet) absorption band and the emission band, using the λ_{max} values. *(g)* In diethyl ether / isopentane / ethanol (2:2:1 v/v). *(h)* The change in lifetime with concentration was too small to estimate a self-quenching rate constant, being scarcely larger than the uncertainty on the measurements. *(i)* The quantum yields of these two complexes will be underestimated, owing to a significant part of the emission falling out of the range of detection of our equipment. Radiative rate constants will be underestimated as a result.
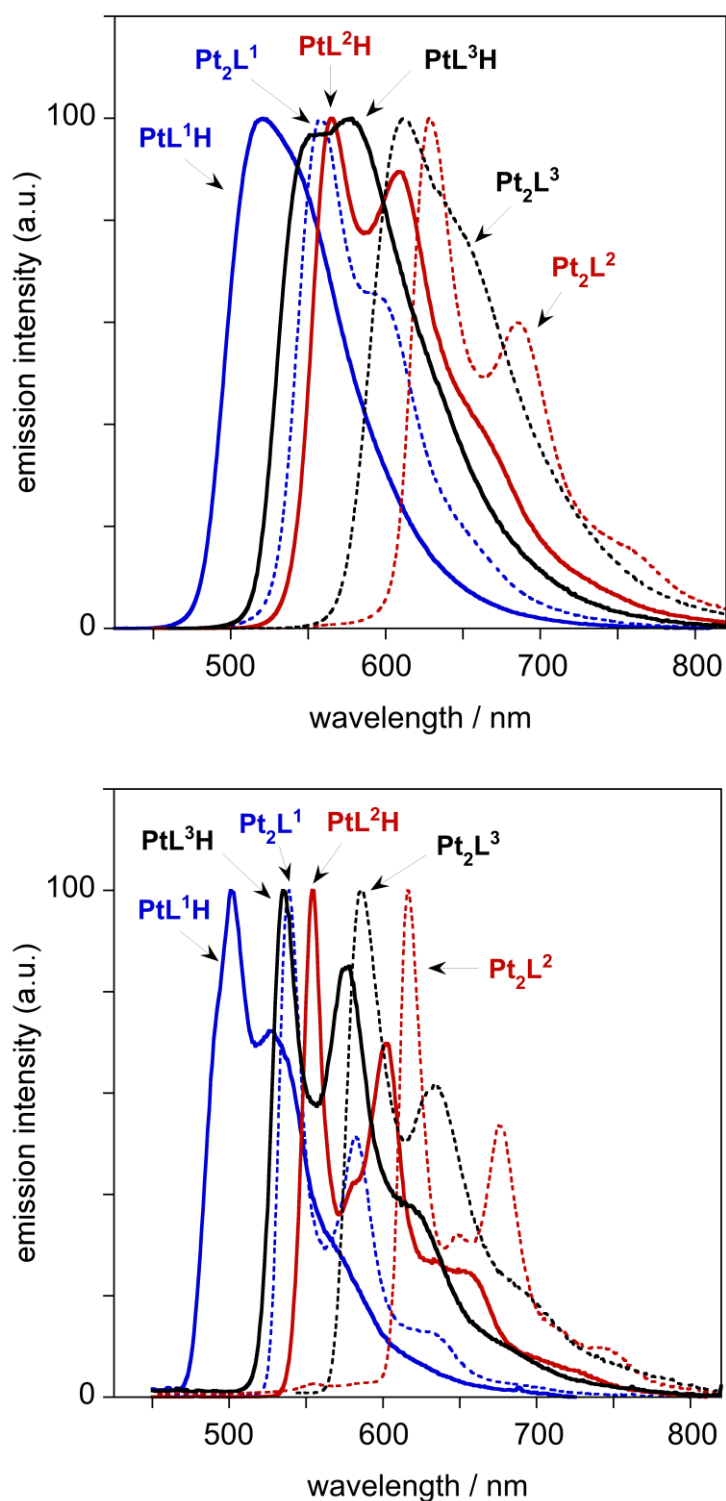
Figure 5 *Top: Normalized emission spectra of PtL$^{1-3}$H (blue, red, and black solid lines respectively, legend as in Figure 2) and of Pt$_2$L$^{1-3}$ (blue, red, and black short-dashed lines respectively) in CH$_2$Cl$_2$ solution at 298 K. Bottom: Corresponding spectra in an EPA glass at 77 K (EPA = diethyl ether / isopentane / ethanol, 2:2:1 v/v).*
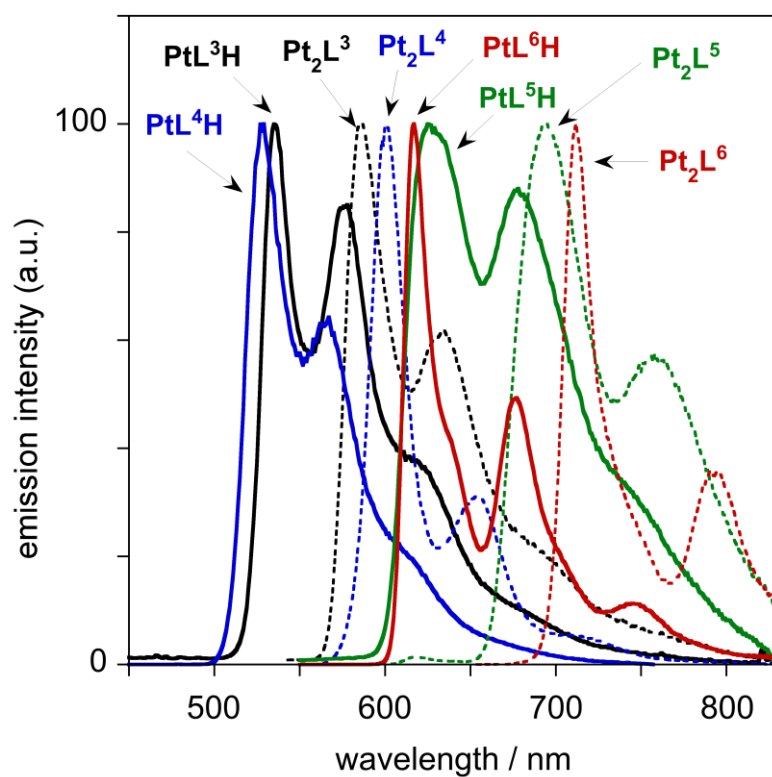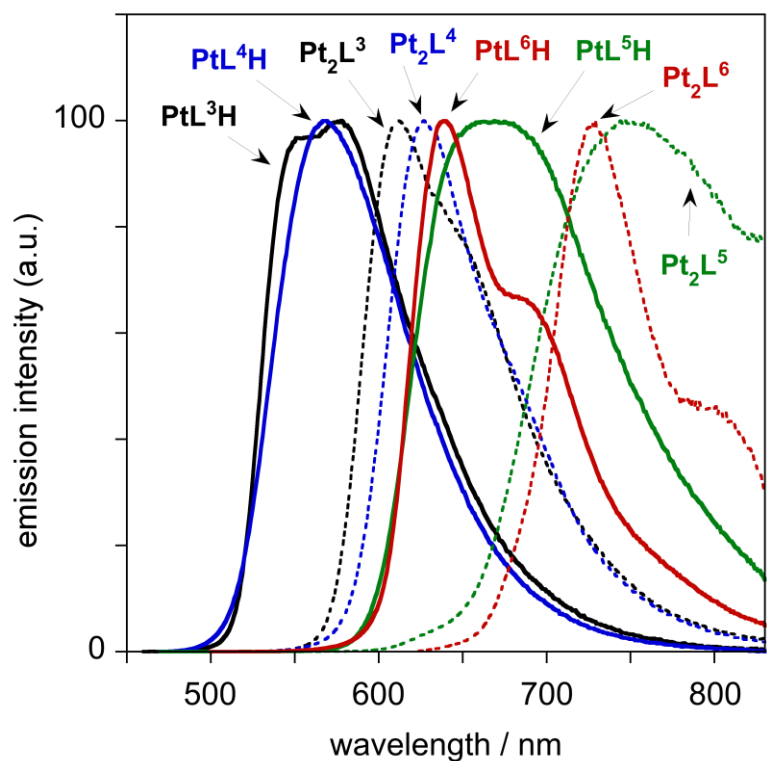
Figure 6 *Top: Normalized emission spectra of Pt$^{3-6}$H (black, blue, green, and red solid lines respectively) and of Pt$_2$L$^{3-6}$ (correspondingly coloured dashed lines) in CH$_2$Cl$_2$ solution at 298 K. Bottom: Corresponding spectra in an EPA glass at 77 K.*

The photoluminescence quantum yields, Φ_{lum}, are high for many of the complexes (Table 2), falling off to < 0.1 only for the most red-emitting complexes, where much of the emission lies in the near infrared. Binuclear complexes such as Pt_2L^2 and Pt_2L^3 are particularly striking in that they have quantum yields of around 0.40 at a λ_{max} that matches well with that of the standard red emitters in RGB displays (e.g. Eu^{3+} phosphors emit at around 617 nm). Indeed, these complexes are brighter than many of the widely-investigated iridium(III) complexes of phenylisoquinoline and benzothienylpyridine ligands,[4a,b,e] which emit in a similar region, and are competitive with quinoxaline-based iridium(III) complexes.[4c,d]
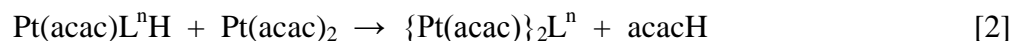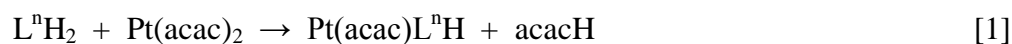
The luminescence lifetimes are of the order of a few microseconds in degassed solution and, for each pair, the lifetime of the binuclear complex is shorter than that of its mononuclear analogue. By estimating the radiative, k_r, and non-radiative, Σk_{nr}, decay rate constants from the quantum yield and lifetime data (Table 2), it can be seen that the introduction of the second metal ion facilitates the radiative decay process by a factor of around 2. Apparently, the emissive transition becomes more allowed in the binuclear complex. Whilst it might be tempting to attribute this effect to additional spin-orbit coupling associated with the second heavy metal ion, it should be noted that the molar absorptivities of the lowest-energy spin-allowed absorption bands are also increased by around two-fold in the binuclear complexes compared to their mononuclear analogues (Table 1 and Figures 2 and 3). Thus, the effect of the second metal ion may be through other mechanisms, such as those related to symmetry, promoting the oscillator strength in absorption and the radiative rate constant in emission.

5. Time-dependent density functional theory (TD-DFT) calculations

Density functional theory calculations have been carried out on all of the compounds shown in Figure 1, but with the dpm ligands truncated to acac in order to facilitate the calculations. It is well-

established that changing from dpm to acac in Pt(N^C)(O^O) complexes has very little influence on the photophysical properties,[11b] and indeed we have confirmed this experimentally in the case of PtL^{1}H and Pt$_2$L^1, where the corresponding acac derivatives have also been studied.[21] The advantage of the dpm ligand is in enhancing solubility. All calculations were performed with Gaussian09W,[xxiii] using the B3LYP functional[xxiv] and 6-31+G(d) basis set for all atoms except Pt, for which the LanL2DZ basis set was employed.[xxv] After full geometry optimization, the visible spectra were calculated by TD-DFT, both in vacuum and in dichloromethane solution using the polarized continuum model for the solvent.[xxvi]

In addition to the spectroscopic analysis, the DFT calculations provide a measure of the relative ground-state stabilities of the mononuclear and dinuclear complexes of a given ligand. For each ligand, the energy changes have been calculated for the hypothetical reactions [1] and [2], generating the mono and dinuclear complexes respectively:

$$L^nH_2 \ + \ Pt(acac)_2 \ \rightarrow \ Pt(acac)L^nH \ + \ acacH \qquad\qquad [1]$$

$$Pt(acac)L^nH \ + \ Pt(acac)_2 \ \rightarrow \ \{Pt(acac)\}_2L^n \ + \ acacH \qquad\qquad [2]$$

The energy changes (ΔE) associated with these reactions are shown in Table 3. The first notable feature is that the introduction of the second Pt center is always more favourable thermodynamically than the first, indicating a synergy in the binding. The trends in complex stabilities for the different ligands can be understood in terms of steric effects: the least sterically hindered ligands L^1H_2 and L^2H_2 give the most stable complexes, and the fused ring systems L^4H_2 and L^6H_2 are a little better than their *ortho*-diphenyl analogues L^3H_2 and L^5H_2, where the complexes show twisting of the ligands to avoid close contacts in the coordinated hydrocarbon rings. The complexes of L^5H_2 and L^6H_2 are the least stable amongst the two series, which can be explained by the close contacts between the O atoms of the acac ligands and the CH groups of the extra ring (closest CH···O contacts are 1.96 – 2.04 Å for L^5H_2

and L^6H_2, compared to $2.35 - 2.58$ Å for L^3H_2 and L^4H_2). This is illustrated for $[\{Pt(acac)\}_2L^5]$ in Figure 7. This steric congestion is also reflected in the calculated Pt–N bond lengths, which are $2.064 - 2.088$ Å for the complexes of L^5H_2 and L^6H_2, significantly longer compared to the range of $2.009 - 2.027$ Å for the complexes of the other four ligands; similarly, the Pt–O bonds *trans* to the metallated carbon are $2.175 - 2.179$ Å for complexes of L^5H_2 and L^6H_2, compared to $2.142 - 2.160$ Å for the other complexes. The calculated Pt–C bond lengths for all 12 complexes are in the range of $1.970 - 2.003$ Å, whilst the Pt–O bonds *trans* to the nitrogen are in the range $2.031 - 2.043$ Å. All of these values are comparable to those obtained in our previous calculations and for experimentally-determined structures of related mononuclear complexes.[21]

Table 3. Calculated gas-phase energy changes for reactions [1] and [2] generating the mono or dinuclear complex.

Species L^n n =	Reaction [1] $\rightarrow Pt(acac)L^nH$ ΔE / kJ mol^{-1}	Reaction [2] $\rightarrow \{Pt(acac)\}_2L^n$ ΔE / kJ mol^{-1}
1	− 13.4	− 42.0
2	− 10.3	− 46.7
3	− 4.2	− 32.8
4	− 6.5	− 33.0
5	+ 25.8	− 12.4
6	+ 14.9	− 23.6
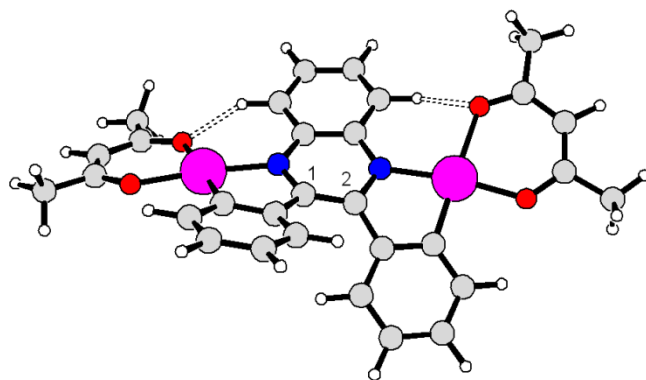
Figure 7 *Calculated structure of Pt$_2$L^5, showing the steric distortion centred on the pyrazine ring. The dotted lines show the close contacts between the C–H groups and O atoms, distance = 2.00 Å. Atom colours: C, grey; N, blue; O, red; Pt, magenta.*

As expected, the proligands whose rings are linked by rotatable C–C bonds are non-planar: the dihedral angles between the heterocyclic and phenyl rings vary from 19° for L^{1}H$_2$ to 42° for L^{3}H$_2$ and L^{5}H$_2$. In the mononuclear complexes of L^{3}H$_2$ and L^{5}H$_2$, and all the complexes of the other ligands, the coordinated rings are essentially co-planar; however, some distortion is observed for the dinuclear complexes of L^{3}H$_2$ and L^{5}H$_2$. This is greatest for Pt$_2$L^5, as shown in Figure 7; the pyrazine ring is twisted, such that carbons 1 and 2 are displaced by 0.12 Å above and below the mean plane of the ring respectively, and the dihedral angle between the two coordinated phenyl rings is 56°. The calculated structure of Pt$_2$L^3 shows slightly smaller distortions: the corresponding carbons in the pyrazine ring are displaced by 0.09 Å out of the mean plane, and the dihedral angle between the two phenyl rings is 43°. This is very similar to the distortions observed in the X-ray crystal structure of the analogous palladium complex [{Pd(acac)}$_2$L^3], for which the equivalent carbons lie 0.15 Å out of the pyrazine mean plane, and the phenyl rings subtend an angle of 46°.[xxvii]

For all these complexes, the calculations reveal that the lowest energy singlet transition (S$_0$→S$_1$) is primarily HOMO→LUMO in nature in each case (Supporting Information). The frontier orbitals for the mono- and dinuclear complexes of L^2, which are shown in Figure 8, are representative of all six

pairs of complexes; frontier orbital plots for all the other complexes are shown in the Supporting Information for reference. For all 12 complexes, the HOMOs are derived mainly from combinations of platinum d-orbitals with π-orbitals of the surrounding ligands, with only small contributions from the pyrazine and pyrimidine rings, whereas these heterocyclic rings are much more important components of the LUMOs. The frontier orbitals of the dinuclear complexes are all symmetrically distributed over both halves of the molecules, whilst those of the mononuclear complexes are all qualitatively similar to their dinuclear counterparts, but of course limited to the one available metal center; this affects the composition of the occupied frontier orbitals more than the virtual orbitals. Nevertheless, the energies of the HOMOs for all 12 complexes are very similar, varying by only 0.077 eV, whereas the energies of the LUMOs vary by 0.784 eV. This is consistent with the conclusions from the experimental electrochemical measurements described in Section 2, which showed little variation in the oxidation potential between the complexes, but a greater range in the reduction potential. Moreover, on going from PtL^nH to Pt_2L^n, the incorporation of the second metal lowers the energy of the LUMO by around 0.3 eV within each pair of complexes (the change is in the range 0.237 to 0.373 eV; see Supporting Information). This observation also correlates well with the electrochemical data, which showed a less negative reduction potential (by around 0.3 eV) for each dinuclear complex compared to its mononuclear analogue (Table 1; the range is 0.23 to 0.38 eV).

There is a good correlation between the energy of the LUMO and energy of the lowest energy singlet transition in the calculated spectra. The calculated absorption spectra are shown in Figure 9, and are in generally good agreement with the experimentally measured spectra. Calculations including the triplet excited states for Pt_2L^1, Pt_2L^2 and Pt_2L^3 in dichloromethane placed the formally spin-forbidden $S_0 \rightarrow T_1$ transitions at 538, 622 and 591 nm respectively, in good agreement with the experimental phosphoresence data discussed in Section 4.
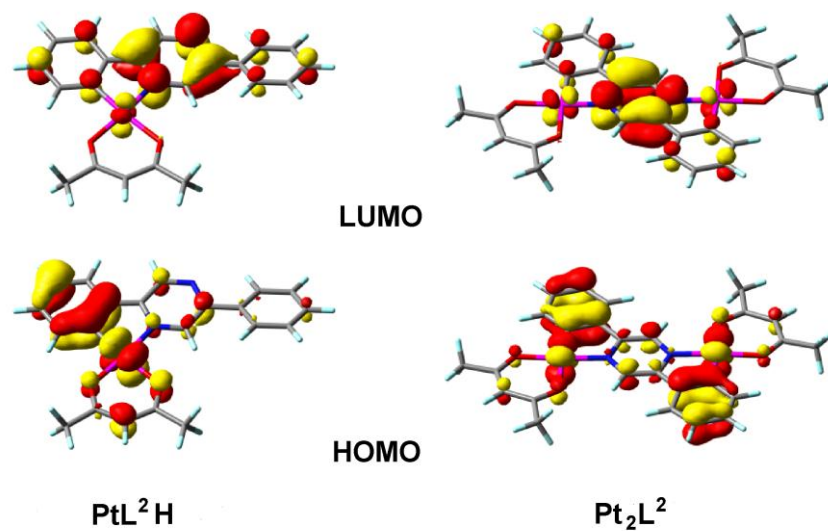
Figure 8 *Frontier orbital diagrams for PtL₂H (left) and Pt₂L² (right).*
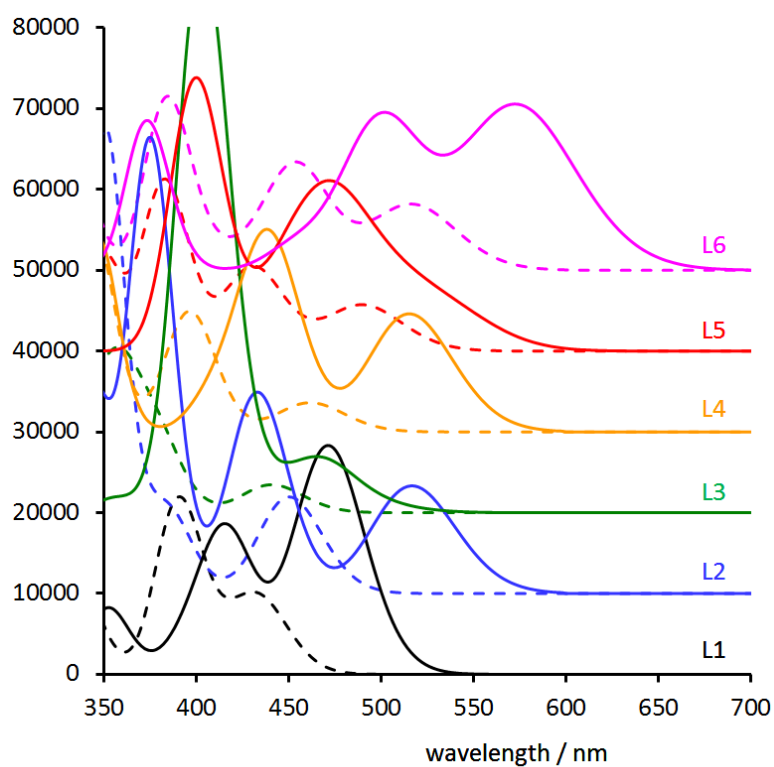
Figure 9 *Simulated UV-visible absorption spectra of the complexes obtained by TD-DFT calculations with a CH₂Cl₂ implicit solvent model. Spectra are displaced vertically for clarity. Spectra of mono- and dinuclear complexes are rendered with broken and solid lines respectively.*

Concluding discussion

We previously showed how 4,6-diphenylpyrimidine can be used as a bridging ligand to prepare dinuclear cyclometallated platinum(II) complexes.[21] The present study shows that diphenylpyrazines can likewise generate dinuclear platinum(II) complexes, through metallation of the two pendent phenyl rings and binding of the metal ions to the two nitrogen atoms of the central heterocycle. Both the 2,3- and 2,5-substituted isomers of diphenylpyrazine can be employed, along with diphenylquinoxaline and derivatives in which the phenyl rings are interlinked through their *ortho* positions. Mono- and di-nuclear complexes can be isolated from a single reaction by chromatographic separation.

The introduction of the second metal ion leads, for all six ligands investigated, to a significant stabilization of the LUMO of around 0.3 eV, according to both cyclic voltammetry and TD-DFT calculations. In contrast, the HOMO energy seems to be influenced rather little. These contrasting effects are intuitively in line with the typical distribution of frontier orbitals in cyclometallated complexes of aryl-heterocycles, in that the ring to which *two* metal ions are bound is the heterocycle, on which the LUMO is predominantly localised. The decreased HOMO–LUMO gap that ensues leads to red-shifted absorption and emission spectra for the dinuclear complexes compared to their mononuclear analogues. Meanwhile, the increased conjugation within the heterocycle on going from a pyrazine through quinoxaline to a phenazine unit (as in L^6) likewise has a much more significant effect on the LUMO, leading to the progressive shift towards the red region observed in the optical spectra.

Of particular interest is the effect of the second metal ion on the radiative rate constant k_r. For all of the systems in which this parameter can be estimated with confidence (Table 2), the value increases upon introduction of the second metal ion, despite the red shift. Normally, for a given type of excited state in structurally related complexes, a decrease in k_r with decreasing energy is anticipated, since the

oscillator strength of a transition is dependent upon ν^3 in the Einstein coefficient for spontaneous emission. However, since the extinction coefficients in the absorption spectra are increased by a comparable factor of around 2-fold, it appears that the effect involved impinges on the singlet states and not just the triplet states. As such, it may not be associated with the higher degree of spin-orbit coupling that might have been expected from the presence of the second heavy metal ion, but rather to facilitation of the transition by other mechanisms.

In summary, dinuclear cyclometallated complexes are shown to offer interesting potential for obtaining phosphorescent materials that both absorb strongly and emit brightly at unusually low energies. Further derivatisation of the diarylpyrazine unit can be confidently expected to lead to further new compounds with opportunities for controlling excited states for contemporary applications, such as in imaging, solar energy conversion, and light-emitting displays.

Experimental

^{1}H and ^{13}C NMR spectra were recorded on JEOL Delta-270 or JEOL ECS-400 spectrometers operating at the frequencies indicated. Chemical shifts (δ) are in ppm, referenced to tetramethylsilane $Si(CH_3)_4$, and coupling constants are in Hertz. Mass spectra were recorded at the EPSRC National Mass Spectrometry Service Centre on a Thermo Scientific LTQ Orbitrap XL Mass Spectrometer using low resolution electrospray (ESI) for or high resolution nano-electrospray (NSI) ionisation techniques. Elemental analyses were carried out using a Carlo Erba 1108 Elemental Analyser controlled with CE Eager 200 software, run in accordance with the manufacturer's instructions and samples weighed using a certified Mettler MX5 Microbalance. Proligands **L^{3}H$_2$** and **L^{5}H$_2$** were purchased from Aldrich and used without additional purification, whilst **L^{4}H$_2$** and **L^{6}H$_2$** were prepared by following literature procedures.[xxviii,xxix]

Absorption spectra were measured on a Biotek Instruments XS spectrometer, using quartz cuvettes of 1 cm path length. Steady-state luminescence spectra were measured using a Jobin Yvon FluoroMax-2 spectrofluorimeter, fitted with a red-sensitive Hamamatsu R928 photomultiplier tube; the spectra

shown are corrected for the wavelength dependence of the detector, and the quoted emission maxima refer to the values after correction. Samples for emission measurements were contained within quartz cuvettes of 1 cm path length modified with appropriate glassware to allow connection to a high-vacuum line. Degassing was achieved via a minimum of three freeze-pump-thaw cycles whilst connected to the vacuum manifold; final vapour pressure at 77 K was $< 5 \times 10^{-2}$ mbar, as monitored using a Pirani gauge. Luminescence quantum yields were determined using $[Ru(bpy)_3]Cl_2$ in degassed aqueous solution as the standard ($\Phi_{lum} = 0.042$ [xxx]); estimated uncertainty in Φ_{lum} is ± 20% or better, except where indicated otherwise.

The luminescence lifetimes of the complexes were measured by time-correlated single-photon counting, following excitation at 374.0 nm with an EPL-375 pulsed-diode laser. The emitted light was detected at 90° using a Peltier-cooled R928 PMT after passage through a monochromator. The estimated uncertainty in the quoted lifetimes is ± 10% or better. Bimolecular rate constants for quenching by molecular oxygen, k_Q, were determined from the lifetimes in degassed and air-equilibrated solution, taking the concentration of oxygen in CH_2Cl_2 at 0.21 atm O_2 to be 2.2 mmol dm^{-3}.[xxxi]

Density Functional Theory Calculations. All DFT calculations were carried out using Gaussian 09W.[23] The B3LYP hybrid functional was used, together with the LanL2DZ basis set for Pt, and 6-31+G(d) for all other atom types. Geometries were fully optimized *in vacuo*. UV-vis spectra were obtained by single point TD-DFT calculations at the optimized geometries, using the same functional and basis sets, either *in vacuo* or with a PCM solvent correction[26] for dichloromethane. The molecular orbitals and spectra were visualized using GaussView 5.0,34 with Gaussian line shapes and an arbitrary half-width at half-height of 1000 cm^{-1} for the latter.

4,6-Diphenylpyrimidine L^{1}H$_2$. Phenylboronic acid (1 g, 8.20 mmol) and 4,6-dichloropyrimidine (469 mg, 3.15 mmol) were dissolved in 1,4-dioxane (25 cm^3) and the reaction mixture was then deaerated by bubbling N_2 through the mixture for 10 minutes. Aqueous K_2CO_3 solution (2M, 9.4 cm^3, 18.8 mmol) and tetrakis(triphenylphosphine)palladium(0) (220 mg, 0.19 mmol) were added and the mixture deaerated for a further 15 minutes. The reaction mixture was then stirred at 95°C under N_2 for 24 h. The solvents were removed under vacuum and DCM (35 cm^3) was added. The organic layer was separated, washed with water (3 × 35 cm^3), dried over MgSO$_4$, filtered and evaporated to dryness. The

product was then purified by column chromatography using silica gel and ethyl acetate / DCM (1:4 ratio) as the eluent; yield 680 mg, 93%. ^{1}H NMR (CDCl$_3$, 270MHz) δ9.31 (1H, d, J = 1.2 Hz), 8.16-8.12 (4H, m), 8.10 (1H, d, J = 1.5 Hz), 7.55-7.50 (6H, m). ^{13}C NMR (CDCl$_3$, 68 MHz) δ_C 164.8, 159.3, 137.2, 131.0, 129.1, 127.3, 112.9. MS (ESI): m/z 233 [M]$^+$. Elemental analysis calcld for C$_{16}$H$_{12}$N$_2$: C 82.73, H 5.21, N 12.06 %; found C 82.85, H 5.33, N 11.92 %.

2,5-Diphenylpyrazine L^{2}H$_2$. Phenylboronic acid (1 g, 8.20 mmol) and 2,5-dibromopyrazine (750 mg, 3.15 mmol) were dissolved in 1,4-dioxane (25 cm^3) and the reaction mixture then deaerated by bubbling N$_2$ through the mixture for 10 minutes. Aqueous K$_2$CO$_3$ solution (2M, 9.0 cm^3, 18.8 mmol) and tetrakis(triphenylphosphine)palladium(0) (6% mol, 220 mg, 0.19 mmol) were added and the mixture was deaerated for a further 15 minutes. The reaction mixture was then stirred at 95°C for 24 h under N$_2$. On cooling, water was added and the resulting precipitate was filtered and dried. The residue was then recrystallized from ethanol; yield 238 mg, 33%. ^{1}H NMR (CDCl$_3$, 270 MHz) δ_H 9.07 (2H, d, J = 0.7 Hz), 8.08–8.03 (4H, m), 7.56-7.46 (6H, m). ^{13}C NMR (CDCl$_3$, 100 MHz) δ_C 150. 8, 141.4, 136.4, 129.9, 129.2, 126.9.

PtL^{1}H and Pt$_2$L^1. A solution of potassium tetrachloroplatinate (1 g, 2.42 mmol) in water (4 cm^3) was added to a stirred solution of L^{1}H$_2$ (375 mg, 1.61 mmol) in acetic acid (80 cm^3). The mixture was heated at reflux under a nitrogen atmosphere for 3 days. The precipitate was filtered off and washed successively with acetic acid (10 cm^3) and ethanol (10 cm^3) to give the dichlorobridged intermediate. A mixture of the intermediate (1.07 g, 1.29 mmol), 2,2,6,6-tetramethyl-3,5-heptanedione (949 mg, 5.16 mmol), aqueous K$_2$CO$_3$ solution (2M, 5 cm^3, 10.32 mmol) and acetone (80 cm^3) was heated at reflux under N$_2$ for 24 h. The solvent was removed by rotary evaporation, the residue was treated with DCM, filtered, and the filtrate was evaporated to dryness. The residue was then purified by column chromatography using silica gel and a mixture of dichloromethane/hexane, 1/2 as the eluent to give both the mononuclear and dinuclear products. **PtL^{1}H,** R$_f$ = 0.1, yield 150 mg, 15 %. ^{1}H NMR (CDCl$_3$, 400 MHz) δ_H 9.62 (1H, d, J = 0.9 Hz), 8.17-8.14 (2H, m), 7.90 (1H, d, J = 0.9 Hz), 7.72 (1H, dd, J = 7.6, 0.8 Hz), 7.64 (1H, dd, J = 7.6, 1.0 Hz), 7.56–7.54 (3H, m), 7.31 (1H, ddd, J = 7.6, 7.6, 1.0 Hz), 7.15 (1H, ddd, J = 7.6, 7.6, 0.8 Hz), 5.84 (1H, s), 1.29 (9H, s), 1.28 (9H, s). HRMS (NSI): m/z 609.2003 [M+H]$^+$. calcld for C$_{27}$H$_{31}$N$_2$O$_2$Pt m/z 609.2007. Elemental analysis calcld for C$_{27}$H$_{30}$N$_2$O$_2$Pt: C 53.20, H 4.96, N 4.60 %; found C 53.31, H 4.92, N 4.49 %. **Pt$_2$L^1,** R$_f$ = 0.2, yield 29 mg, 1.8 %. ^{1}H NMR (CDCl$_3$, 400 MHz) δ_H 9.68 (1H, s), 7.71 (2H, br.d, J = 7.6 Hz), 7.70 (1H, s), 7.62

(2H, br.d, J = 7.6 Hz), 7.34 (2H, br.t, J = 7.6 Hz), 7.17 (2H, br.t, J = 7.6 Hz), 5.84 (2H, s), 1.28 (18H, s) 1.26 (18H, s).   HRMS (NSI): m/z 985.2934 [M+H]$^+$. calcld for $C_{38}H_{48}N_2O_4Pt_2H$ m/z 985.2941. Elemental analysis calcld for $C_{38}H_{48}N_2O_4Pt_2$: C 46.24, H 4.90, N 2.84 %; found C 46.30, H 5.25, N 2.64%.

PtL^{2}H and Pt$_2$L^2. A solution of potassium tetrachloroplatinate (896 mg, 2.16 mmol) in water (4 cm^3) was added to a stirred solution of L^2H_2 (250 mg, 1.08 mmol) in acetic acid (80 cm^3). The mixture was heated at reflux under N_2 for 3 days. The precipitate was filtered off and washed consecutively with acetic acid (10 cm^3) and ethanol (10 cm^3) and dried to give the dichlorobridged dimer. A mixture of the dimer (680 mg, 1.32 mmol), 2,2,6,6-tetramethyl-3,5-heptanedione (972 mg, 5.28 mmol), aqueous K_2CO_3 solution (2M, 5 cm^3, 10.56 mmol) and acetone (80 cm^3) was heated at reflux under N_2 for 24 h. Acetone was removed by rotary evaporation and the residue was then washed with water, filtered and dried. The solid was purified by column chromatography using silica gel and dichloromethane as an eluent to give both the mononuclear and dinuclear products. For **PtL^{2}H**, R_f = 0.6, yield 230 mg, 35 %. ^{1}H NMR (CDCl$_3$, 400 MHz) δ_H 9.54 (1H, d, J = 1.2 Hz, $^3J_{H-Pt}$ = 46 Hz), 8.95 (1H, d, J = 1.2 Hz, $^4J_{H-Pt}$ = 13 Hz), 8.06–8.01 (2H, m), 7.70 (1H, dd, J = 7.8, 1.6 Hz), 7.60 (1H, dd, J = 7.8, 1.6 Hz), 7.58–7.48 (3H, m), 7.29 (1H, ddd, J = 7.4, 7.4, 1.2 Hz), 7.17 (1H, ddd, J = 7.4, 7.4, 1.2 Hz), 5.86 (1H, s), 1.34 (9H, s), 1.31 (9H, s). HRMS (NSI): m/z 609.2003 [M+H]$^+$. calcld for $C_{27}H_{31}N_2O_2PtH$ m/z 609.2007. Elemental analysis calcld for $C_{27}H_{30}N_2O_2Pt$: C 53.20, H 4.96, N 4.60 %; found C 52.52, H 4.47, N 4.15 %. For **Pt$_2$L$_2$**, R_f = 0.9, yield 150 mg, 15 %. ^{1}H NMR (CDCl$_3$, 400 MHz) δ_H 9.44 (2H, s), 7.72 (2H, dd, J = 6.7, 1.5 Hz), 7.43 (2H, dd, J = 6.7, 1.5 Hz), 7.29 (2H, ddd, J = 7.7, 7.7, 1.5 Hz), 7.17 (2H, ddd, J = 7.7, 7.7, 1.5 Hz), 5.88 (2H, s), 1.37 (18H, s), 1.30 (18H, s). HRMS (NSI): m/z 985.2940 [M+H]$^+$. calcld for $C_{38}H_{48}N_2O_4Pt_2H$ m/z 985.2941. Elemental analysis calcld for $C_{38}H_{48}N_2O_4Pt_2$: C 46.24, H 4.90, N 2.84 %; found C 46.36, H 5.27, N 2.60%.

PtL^{3}H. A solution of potassium tetrachloroplatinate (270 mg, 0.65 mmol) in water (2 cm^3) was added to a stirred solution of L^3H_2 (150 mg, 0.65 mmol) in acetic acid (60 cm^3). The mixture was heated at reflux under an argon atmosphere for 19 h. The precipitate was filtered off and washed successively with acetic acid (10 cm^3) and ethanol (10 cm^3) and dried to give the dichlorobridged dimer. A mixture of the dimer (150 mg, 0.30 mmol), 2,2,6,6-tetramethyl-3,5-heptanedione (166 mg, 0.90 mmol), aqueous K_2CO_3 solution (2M, 1 cm^3, 1.8 mmol) and ethoxyethanol (70 cm^3) was heated at reflux under argon for 15 h. The solvent was evaporated and the solid washed in water (70 cm^3). The solid was

then filtered, dried, and purified by column chromatography using silica gel and dichloromethane as the eluent; R_f = 0.4 yield 140 mg, 35 %. ^{1}H NMR (CDCl$_3$, 400 MHz) δ_H 9.10 (1H, d, J = 3.4 Hz, $^3J_{H\text{-}Pt}$ = 47 Hz), 8.33 (1H, d, J = 4.5 Hz), 7.69 (1H, dd, J = 7.9, 1.4 Hz), 7.57–7.49 (5H, m), 7.13 (1H, ddd, J = 7.8, 7.2, 1.8 Hz), 6.75-6.23 (2H, m), 5.84 (1H, s), 1.29 (9H, s), 1.28 (9H, s). MS (ESI): m/z 609 [M+H]$^+$. Elemental analysis calcld for C$_{27}$H$_{30}$N$_2$O$_2$Pt: C 53.20, H 4.96, N 4.60 %; found C 53.64, H 5.18, N 4.52 %.

Pt$_2$L^3. A solution of potassium tetrachloroplatinate (540 mg, 1.30 mmol) in water (4 cm^3) was added to a stirred solution of L^{3}H$_2$ (150 mg, 0.65 mmol) in acetic acid (60 cm^3). The mixture was heated at reflux under N$_2$ for 24 h. The precipitate was filtered off and washed successively with acetic acid (10 cm^3) and ethanol (10 cm^3) and dried to give the dichlorobridged dimer. A mixture of the dimer (200 mg, 0.26 mmol), 2,2,6,6-tetramethyl-3,5-heptanedione (144 mg, 0.78 mmol), aqueous K$_2$CO$_3$ solution (2M, 1 cm^3, 1.56 mmol) and ethoxyethanol (70 cm^3) was heated under reflux under nitrogen for 15 h. The solvent was evaporated and the solid washed with water (70 cm^3). The solid was then filtered off and dried. The product was purified by column chromatography using silica gel and dichloromethane as an eluent; R_f = 0.9 yield 60 mg, 9 %. ^{1}H NMR (CDCl$_3$, 400 MHz) δ_H 8.69 (2H, s), 8.03 (2H, dd, J = 8.5, 2.0 Hz), 7.73 (2H, dd, J = 8.5, 2.0 Hz), 7.31-7.25 (2H, m), 7.00 (2H, ddd, J = 7.6, 7.8, 1.8 Hz), 5.86 (2H, s), 1.31 (18H, s), 1.30 (18H, s). MS (ESI): m/z 985 [M+H]$^+$. Elemental analysis calcld for C$_{38}$H$_{48}$N$_2$O$_4$Pt$_2$: C 46.24, H 4.90, N 2.84 %; found C 46.31, H 5.05, N 2.79 %.

PtL^{4}H and Pt$_2$L^4. A solution of potassium tetrachloroplatinate (452 mg, 1.09 mmol) in water (2 cm^3) was added to a stirred solution of L^{4}H$_2$ (250 mg, 1.09 mmol) in acetic acid (75 cm^3). The mixture was heated at reflux under N$_2$ for 24 h. The precipitate was filtered off and washed successively with acetic acid (10 cm^3) and ethanol (10 cm^3) and dried to give the dichlorobridged dimer. A mixture of the dimer (270 mg, 0.55 mmol), 2,2,6,6-tetramethyl-3,5-heptanedione (304 mg, 1.65 mmol), aqueous K$_2$CO$_3$ solution (2M, 2 cm^3, 3.3 mmol) and acetone (70 cm^3) was heated under reflux, under N$_2$ for 23 h. The mixture was filtered and water (70 cm^3) was added to the filtrate. The precipitated solid was filtered off, washed with water and dried. The product was then purified by column chromatography using silica gel and dichloromethane as the eluent to give both the mononuclear and dinuclear products. For **PtL^{4}H**, Rf = 0.7, yield 100 mg, 15%. ^{1}H NMR (CDCl$_3$, 400 MHz) δ_H 9.13 (1H, dd, J = 7.7, 1.3 Hz), 9.09 (1H, d, J = 3.4 Hz), 8.75 (1H, d, J = 3.4 Hz), 8.60 (1H, dd, J = 8.2, 1.3 Hz), 8.19 (1H, dd, J = 8.2, 1.3 Hz), 7.86–7.63 (4H, m), 5.91 (1H, s), 1.18, (18H, s). MS (ESI): m/z 607 [M$^+$H]$^+$. Elemental

analysis calcld for $C_{27}H_{28}N_2O_2Pt$: C 53.37, H 4.64, N 4.61 %; found C 53.65, H 4.75, N 4.48 %. For **Pt₂L⁴**, R_f = 0.9, yield 50 mg, 5 %. ¹H NMR (CDCl₃, 400 MHz) δ_H 8.69 (2H, s), 8.09 (2H, d, *J* = 7.6 Hz), 7.75 (2H, d, *J* = 8.4 Hz), 7.62 (2H, t, *J* = 8.0, 7.6 Hz), 5.91 (2H, s), 1.36 (18H, s), 1.35 (18H, s). MS (ESI): *m/z* 982 [M+ H]⁺. Elemental analysis calcld for $C_{38}H_{46}N_2O_4Pt$: C 46.69, H 4.95, N 2.81 %; found C 46.86, H 4.87, N 2.82 %.

PtL⁵H. Under N_2 atmosphere, L^5H_2 (220 mg, 0.78 mmol) and potassium tetrachloroplatinate (420 mg, 1.01 mmol) were dissolved in acetic acid (50 cm³) and the mixture was heated at reflux overnight. The mixture was cooled to room temperature and the black solid was filtered off, washed with ethanol (20 cm³) and air dried. The crude product was added to a solution of 2,2,6,6-tetramethyl-3,5-heptanedione (432 mg, 2.34 mmol) in acetone (60 cm³), followed by aqueous K_2CO_3 solution (2M, 5 cm³). The mixture was heated at reflux overnight. Acetone was removed under reduced pressure and the crude product was dissolved in DCM. The organic layer was washed with brine and dried with $MgSO_4$. The solvent was removed under vacuum and the product was then purified by column chromatography using silica gel and CHCl₃. R_f = 0.4, yield 231 mg, 45%. ¹H NMR (CDCl₃, 400 MHz) δ_H 9.42 (1H, dd, *J* = 8.2 Hz, *J* = 1.4 Hz), 8.09 (1H, dd, *J* = 7.6 Hz, *J* = 1.6 Hz), 7.83 (1H, d, *J* = 7.8 Hz), 7.68-7.76 (4H, m), 7.50-7.56 (3H, m), 7.14 (1H, m), 6.71-6.77 (2H, m), 5.93 (1H, s), 1.32 (9H, s), 1.27 (9H, s). MS (ESI): *m/z* 659 [M+H]⁺. Elemental analysis calcld for $C_{31}H_{32}N_2O_2Pt$: C 56.44, H 4.89, N 4.25 %; found C 56.84, H 5.12, N 4.08 %.

Pt₂L⁵. Under N_2 atmosphere, PtL⁵H (200 mg, 0.3 mmol) and potassium tetrachloroplatinate (415 mg, 0.36 mmol) were dissolved in acetic acid (40 cm³) and the mixture was heated at reflux 15 h. The mixture was cooled to room temperature and the black solid was filtered off, washed with ethanol (20 cm³) and air dried. The crude product was added to a solution of 2,2,6,6-tetramethyl-3,5-heptanedione (74 mg, 0.4 mmol) in acetone (50 cm³), followed by aqueous K_2CO_3 solution (2M, 5 cm³). The mixture was heated at reflux for 16 h. Acetone was removed under reduced pressure and the crude product dissolved in DCM. The organic layer was washed with brine, dried over $MgSO_4$, filtered and evaporated to dryness. The residue was then purified by column chromatography using silica gel and CH₃Cl as the eluent to give the product; R_f = 0.8 yield 102 mg, 33%. ¹H NMR (CDCl₃, 400 MHz) δ_H 9.49 (2H, m), 8.00 (2H, br.d, *J* = 10.0 Hz), 7.85 (2H, dd, *J* = 12.0 Hz, *J* = 2.4 Hz), 7.64 (2H, m), 7.26 (2H, ddd, *J* = 12.0 Hz, *J* = 11.6 Hz, *J* = 1.6 Hz), 7.00 (2H, ddd, *J* = 11.6 Hz, *J* = 10.4 Hz, *J* = 2.4 Hz),

5.96 (2H, s), 1.34 (18H, s), 1.28 (18H, s). MS (ESI): m/z 1035 [M+ H]$^+$. Elemental analysis calcld for C$_{42}$H$_{50}$N$_2$O$_4$Pt$_2$: C 48.64, H 4.86, N 2.70 %; found C 48.86, H 5.38, N 2.48 %

PtL^{6}H and **Pt$_2$L^6.** A mixture of L^{6}H$_2$ (93 mg, 0.33 mmol), potassium tetrachloroplatinate (150 mg, 0.4 mmol) and acetic acid (35 cm^3) were heated at reflux under nitrogen for 14 h. The mixture was allowed to cool to room temperature and the black solid was filtered off, washed with ethanol (20 cm^3) and air dried. The crude product was added to a solution of 2,2,6,6-tetramethyl-3,5-heptanedione (431 mg, 2.34 mmol) in acetone (60 cm^3), followed by aqueous K$_2$CO$_3$ solution (2M, 5 cm^3). The mixture was heated at reflux for 14 h. Acetone was removed under reduced pressure, and DCM (30 cm^3) and brine (15 cm^3) were added. The organic layer was dried over MgSO$_4$ and filtered. The solvent was removed by rotary evaporation and the residue was then purified by column chromatography using silica gel and CHCl$_3$ / hexane, 7/3 v/v, as the eluent to give both the mononuclear and dinuclear products. For **PtL^{6}H**, R$_f$ = 0.7, yield 24 mg, 11%. ^{1}H NMR (CDCl$_3$, 400 MHz) δ$_H$ 10.07 (1H, dd, J = 8.7 Hz, J = 1.4 Hz), 9.31 (1H, dd, J = 9.2 Hz, J = 1.4 Hz), 8.50 (1H, d, J = 7.8 Hz), 8.36 (1H, dd, J = 8.7 Hz, J = 1.4 Hz), 8.12 (1H, d, J = 7.8 Hz), 7.99 (1H, d, J = 6.9 Hz), 7.69-7.92 (4H, m), 7.62 (1H, t, J = 7.8 Hz), 5.99 (1H, s), 1.38 (9H, s), 1.37 (9H, s). MS (ESI): m/z 657 [M$^+$ H]$^+$. Elemental analysis calcld for C$_{31}$H$_{30}$N$_2$O$_2$Pt: C 56.61, H 4.60, N 4.26 %; found C 56.59, H 4.63, N 4.18 %. For **Pt$_2$L^6**, R$_f$ = 0.8, yield 2 mg, 0.6%. ^{1}H NMR (CDCl$_3$, 400 MHz) δ$_H$ 10.15 (2H, m), 8.06 (2H, d, J = 7.8 Hz), 7.96 (2H, d, J = 7.3 Hz), 7.87 (2H, m), 7.61 (2H, t, J = 7.8 Hz), 5.99 (2H, s), 1.38 (18H, s), 1.37 (18H, s). MS (ESI): m/z 1033 [M+ H]$^+$.

¶ **Supporting Information Available:** ^{1}H NMR; data from DFT calculations; frontier orbital plots for all complexes generated by TD-DFT calculations. This material is available free of charge via the Internet at http://pubs.acs.org.

References

1. Yersin, H., Ed.; *Highly Efficient OLEDs with Phosphorescent materials*; Wiley-VCH: Weinheim, Germany, 2008.
2. Buckley, A., Ed.; *Organic light-emitting diodes: Materials, devices and applications*; Woodhead: Cambridge, 2013, in press.
3. (a) D'Andrade, B.W.; Forrest, S.R. *Adv. Mater.* **2004**, *16*, 1585. (b) So, F.; Kido, J.; Burrows, P.

MRS Bulletin, **2008**, *7*, 663. (c) Sun, Y.; Forrest, S. R. *Appl. Phys. Lett.* **2007**, *91*, 263503.

4. (a) Lamansky, S.; Djurovich, P.; Murphy, D.; Abdel-Razzaq, F.; Lee, H. E.; Adachi, C.; Burrows, P. E.; Forrest, S. R.; Thompson, M. E. *J. Am. Chem. Soc.* **2001**, *123*, 4304. (b) Tsuboyama, A.; Iwawaki, H.; Furugori, M.; Mukaide, T.; Kamatani, J.; Igawa, S.; Moriyama, T.; Miura, S.; Takiguchi, T.; Okada, S.; Hoshini, M.; Ueno, K. *J. Am. Chem. Soc.* **2003**, *125*, 12971. (c) Su, Y.-J.; Huang, H.-L.; Li, C.-L.; Chien, C.-H.; Tao, Y.-T.; Chou, P.-T.; Datta, S.; Liu, R.-S. *Adv. Mater.* **2003**, *15*, 224. (d) Hwang, F.-M.; Chen, H.-Y.; Chen, P.-S.; Liu, C.-S.; Chi, Y.; Shu, C.-F.; Wu, F.-I.; Chou, P.-T.; Peng, S.-M.; Lee, G.-H. *Inorg. Chem.* **2005**, *44*, 1344. (e) Bronstein, H.; Finlayson, C. E.; Kirov, K. R.; Friend, R. H.; Williams, C. K. *Organometallics*, **2008**, *27*, 2980.

5. (a) Fernandez-Moreira, V.; Thorp-Greenwood, F. L.; Coogan, M. P. *Chem. Commun.* **2010**, *46*, 186. (b) Lo, K.K.-W.; Li, S.P.-Y.; Zhang, K.-Y. *New J. Chem.* **2011**, *35*, 265. (c) Zhao, Q.; Huang, C.; Li, F. *Chem. Soc. Rev.* **2011**, *40*, 2508. (d) Baggaley, E.; Weinstein, J.A.; Williams, J.A.G. *Coord. Chem. Rev.* **2012**, *256*, 1762.

6. Wang, L.V.; Wu, H. *Biomedical Optics: Principles and Imaging*; John Wiley: Hoboken, NJ, 2007.

7. (a) Ardo, S.; Meyer, G. J. *Chem. Soc. Rev.* **2009**, *38*, 115. (b) Hagfeldt, A.; Boschloo G.; Sun, L.; Kloo, L.; Pettersson, H. *Chem. Rev.* **2010**, *110*, 6595. (c) Abbotto, A.; Manfredi, N. *Dalton Trans.* **2011**, *40*, 12421.

8. Juris, A.; Balzani, V.; Barigelletti, F.; Campagna, S.; Belser, P.; Von Zelewsky, A. *Coord. Chem. Rev.* **1988**, *84*, 85.

9. For reviews, see: (a) Dixon, I. M.; Collin, J.-P.; Sauvage, J.-P.; Flamigni, L.; Encinas, S.; Barigelletti, F. *Chem. Soc. Rev.* **2000**, *29*, 385. (b) Lowry, M. S.; Bernhard, S. *Chem. Eur. J.* **2006**, *12*, 7970. (c) Flamigni, L.; Barbieri, A.; Sabatini, C.; Ventura, B.; Barigelletti, F. *Top. Curr. Chem.* **2007**, *281*, 143. (d) Wong, W.-Y.; Ho, C. L. *J. Mater. Chem.* **2009**, *19*, 4457. (e) Williams, J. A. G.; Wilkinson, A. J.; Whittle, V. L. *Dalton Trans.* **2008**, 2081. (f) Chi, Y.; Chou, P.-T. *Chem. Soc. Rev.* **2010**, *39*, 638. (g) Liu, Z.; Bian, Z.; Huang, C. *Top. Organomet. Chem.* **2010**, *28*, 113. (h) You, Y.; Nam, W. *Chem. Soc. Rev.* **2012**, *41*, 7061.

10. (a) Baldo, M. A.; O'Brien, D. F.; You, Y.; Shoustikov, A.; Sibley, S.; Thompson, M. E.; Forrest, S. R. *Nature* **1998**, *395*,151. (b) Lamansky, S.; Djurovich, P.; Murphy, D.; Abdel-Razzaq, F.; Lee, H.-E.; Adachi, C.; Burrows, P. E.; Forrest, S. R.; Thompson, M. E. *J. Am. Chem. Soc.* **2001**, *123*, 4304. (b) Grushin, V. V.; Herron, N.; LeCloux, D. D.; Marshall, W. J.; Petrov, V. A.; Wang, Y. *Chem. Commun.* **2001**, *16*, 1494. (c) Tsuboyama, A.; Iwawaki, H.; Furugori, M.; Mukaide, T.; Kamatani, J.; Igawa, S.; Moriyama, T.; Miura, S.; Takiguchi, T.; Okada, S.; Hoshino, M.; Ueno, K. *J. Am. Chem. Soc.* **2003**, *125*, 12971. (d) Tamayo, A. B.; Alleyne, B. D.; Djurovich, P. I.; Lamansky, S.; Tsyba, I.; Ho, N. N.; Bau, R.; Thompson, M. E. *J. Am. Chem. Soc.* **2003**, *125*, 7377. (e) Zhao, Q.; Jiang, C.-Y.; Shi, M.; Li, F.-Y.; Yi, T.; Cao, Y.; Huang, C.-H. *Organometallics* **2006***, 25*, 3631. (f) Xu, M. L.; Wang, G. Y.; Zhou, R.; An, Z. W.; Zhou, Q.; Li, W. L. *Inorg. Chim. Acta.* **2007**, *360*, 3149.

11. For reviews, see: (a) Lai, S.-W.; Che, C.-M. *Top. Curr. Chem.* **2004**, *241*, 27. (b) Williams, J. A. G. *Top. Curr. Chem.* **2007**, *281*, 205. (c) Williams, J. A. G.; Develay, S.; Rochester, D. L.; Murphy, L. *Coord. Chem. Rev.* **2008**, *252*, 2596. (d) Murphy, L.; Williams, J.A.G. *Top. Organomet. Chem.* **2010**, *28*, 75.

12. (a) Balashev, K. P.; Puzyk, M. V.; Kotlyar, V. S.; Kulikova, M.V. *Coord. Chem. Rev.* **1997**, *159*, 109. (b) Brooks, J.; Babayan, Y.; Lamansky, S.; Djurovich, P. I.; Tsyba, I.; Bau, R.; Thompson, M. E. *Inorg. Chem.* **2002**, *41*, 3055. (c) Yin, B. L.; Niemeyer, F.; Williams, J. A. G.; Jiang, J.; Boucekkine, A.; Toupet, L.; Le Bozec, H.; Guerchais, V. *Inorg. Chem.* **2006**, *45*, 8584. (d) Niedermair, F.; Kwon, O.; Zojer, K.; Kappaun, S.; Trimmel, G.; Mereiter, K.; Slugovc, C. *Dalton Trans.* **2008**, 4006. (e) Ghedini, M.; Pugliese, T.; La Deda, M.; Godbert, N.; Aiello, I.; Amati, M.;

Belviso, S.; Lelj, F.; Accorsi, G.; Barigelletti, F. *Dalton Trans.* **2008**, 4303. (f) Chang, S.-Y.; Cheng, Y.-M.; Chi, Y.; Lin, Y.-C.; Jiang, C.-M.; Lee, G.-H.; Chou, P.-T. *Dalton Trans.* **2008**, 6901. (g) Wong, W.-Y.; Ho, C.-L. *J. Mater. Chem.* **2009**, *19*, 4457. (h) Liu, J.; Yang, C.-J.; Cao, Q.-Y.; Xu, M.; Wang, J.; Peng, H.-N.; Tan, W.-F.; Lue, X.-X.; Gao, X.-C. *Inorg. Chim. Acta* **2009**, *362*, 575. (i) Santoro, A.; Whitwood, A. C.; Williams, J. A. G.; Kozhevnikov, V. N.; Bruce, D. W. *Chem. Mater.* **2009**, *21*, 3871. (j) Zhou, G.; Wang, Q.; Ho, C.-L.; Wong, W.-Y.; Ma, D.; Wang, L. *Chem. Commun.* **2009**, 3574. (k) Feng, K.; Zuniga, C.; Zhang, Y.-D.; Kim, D.; Barlow, S.; Marder, S. R.; Brédas, J. L.; Weck, M. *Macromolecules* **2009**, *42*, 6855. (l) Zhou, G. J.; Wang, Q.; Wang, X. Z.; Ho, C. L.; Wong, W. Y.; Ma, D. G.; Wang, L. X.; Lin, Z. Y. *J. Mater. Chem.* **2010**, *20*, 7472. (m) Vezzu, D. A. K.; Deaton, J. C.; Jones, J. S.; Bartolotti, L. C.; Harris, F.; Marchetti, A. P.; Kondakova, M.; Pike, R. D.; Huo, S. *Inorg. Chem.* **2010**, *49*, 5107. (n) Wu, W. H.; Wu, W. T.; Ji, S. M.; Guo, H. M.; Song, P.; Han, K. L.; Chi, L. N.; Shao, J. Y.; Zhao, J. Z. *J. Mater. Chem.* **2010**, *20*, 9775. (o) Chan, J.C.-H.; Lam, W.H.; Wong, H.-L.; Zhu, N.Y.; Wong. W.-T.; Yam, V.W.-W. *J. Am. Chem. Soc.* **2011**, *133*, 12690.

13. (a) Rausch, A. F.; Homeier, H. H. H.; Djurovich, P. I.; Thompson, M. E.; Yersin, Y. *Proc. SPIE.* **2007**, *6655*, F6550. (b) Yersin H.; Rausch, A. F.; Czerwieniec, R.; Hofbeck, T.; Fischer, T. *Coord. Chem. Rev.* **2011**, *255*, 21.

14. Hay, P.J. *J. Phys. Chem. A* **2002**, *106*, 1634.

15. Okada, S.; Okinaka, K.; Iwawaki, H.; Furugori, M.; Hashimoto, M.; Mukaide, T.; Kamatani, J.; Igawa, S.; Tsuboyama, A.; Takiguchi, T.; Ueno, K. *Dalton Trans*. **2005**, 1583.

16. Lamansky, S.; Djurovich, P.; Murphy, D.; Abdel-Razzaq, F.; Kwong, R.; Tsyba, I.; Bortz, M.; Mui, B.; Bau, R.; Thompson, M.E. *Inorg. Chem.* **2001**, *40*, 1704.

17. Lepeltier, M.; Le Bozec, H.; Guerchais, V.; Lee, T. K.-M.; Lo, K. K.-W. *Organometallics* **2005**, *24,* 6069.

18. (a) Chou, P.T.; Chi, Y.; Chung, M.W.; Lin, C.C. *Coord. Chem. Rev.* **2011**, *255*, 2653. (b) Chen, Y.L.; Li, S.W.; Chi, Y.; Cheng, Y.M.; Pu, S.C.; Yeh, Y.S.; Chou, P.T. *ChemPhysChem* **2005**, *6*, 2012.

19. Kozhevnikov, D. N.; Kozhevnikov, V. N.; Shafikov, M. Z.; Prokhorov, A. M.; Bruce, D. W.; Williams, J. A. G. *Inorg. Chem.* **2011**, *50*, 3804.

20. Wu, S.H.; Burkhardt, S.E.; Yao, J.; Zhong, Y.W.; Abruña, H.D. *Inorg. Chem.* **2011**, *50*, 3959.

21. Kozhevnikov, V. N.; Durrant, M. C.; Williams, J. A. G. *Inorg. Chem.* **2011**, *50*, 6304.

xxii. Williams, J. A. G.; Beeby, A.; Davies, E. S.; Weinstein, J. A.; Wilson, C. *Inorg. Chem.* **2003**, *42*, 8609.

xxiii. Frisch, M. J.; Trucks, G. W.; Schlegel, H. B.; Scuseria, G. E.; Robb, M. A.; Cheeseman, J. R.; Scalmani, G.; Barone, V.; Mennucci, B.; Petersson, G. A.; Nakatsuji, H.; Caricato, M.; Li, X.; Hratchian, H. P.; Izmaylov, A. F.; Bloino, J.; Zheng, G.; Sonnenberg, J. L.; Hada, M.; Ehara, M.; Toyota, K.; Fukuda, R.; Hasegawa, J.; Ishida, M.; Nakajima, T.; Honda, Y.; Kitao, O.; Nakai, H.; Vreven, T.; Montgomery, Jr., J. A.; Peralta, J. E.; Ogliaro, F.; Bearpark, M.; Heyd, J. J.; Brothers, E.; Kudin, K. N.; Staroverov, V. N.; Kobayashi, R.; Normand, J.; Raghavachari, K.; Rendell, A.; Burant, J. C.; Iyengar, S. S.; Tomasi, J.; Cossi, M.; Rega, N.; Millam, J. M.; Klene, M.; Knox, J. E.; Cross, J. B.; Bakken, V.; Adamo, C.; Jaramillo, J.; Gomperts, R.; Stratmann, R. E.; Yazyev, O.; Austin, A. J.; Cammi, R.; Pomelli, C.; Ochterski, J. W.; Martin, R. L.; Morokuma, K.; Zakrzewski, V. G.; Voth, G. A.; Salvador, P.; Dannenberg, J. J.; Dapprich, S.; Daniels, A. D.; Farkas, Ö.; Foresman, J. B.; Ortiz, J. V.; Cioslowski, J.; Fox, D. J. *Gaussian 09W*, Version 7.0; Gaussian, Inc.: Wallingford, CT, 2009.

xxiv. Becke, A. *Chem. Phys.* **1993**, 98, 5648.

xxv.Hay, P.; Wadt W. *J. Chem. Phys.* **1985**, 82, 270.

xxvi. Cossi, K.; Scalmani, G.; Rega, N.; Barone, V. *J. Chem. Phys.* **2002**, *117*, 43.

xxvii. Steel, P. J; Caygill, G. B. *J. Organomet. Chem.* **1990**, *395*, 359.

xxviii. Mason, A. T. *Berichte der deutscehn chemischen Gesellschaft* **1886**, *19*, 112.

xxix. Minsky, A.; Cohen, Y.; Rabinovitz, M. *J. Am. Chem. Soc.* **1985**, *107*, 1501.

xxx. Van Houten, J.; Watts, R.J. *J. Am. Chem. Soc.* **1976**, *98*, 4853.

xxxi. Murov, S.L.; Carmichael, I.; Hug, G.L. *Handbook of Photochemistry,* 2nd ed., Marcel Dekker: New York, 1993.